Systematic Study of Aluminum Corrosion in Ionic Liquid Electrolytes for Sodium-Ion Batteries: Impact of Temperature and Concentration

Huazhen Liu, Jinkwang Hwang,[*] Kazuhiko Matsumoto,[*] Rika Hagiwara1

Graduate School of Energy Science, Kyoto University, Yoshida-honmachi, Sakyo-ku, Kyoto 606-8501, Japan

*Corresponding Authors

E-mail: k-matsumoto@energy.kyoto-u.ac.jp (K.M.)

hwang.jinkwang.5c@kyoto-u.ac.jp (J.H.)

ABSTRACT

The development of next-generation sodium-ion batteries utilizing sulfonylamide-based electrolytes is significantly encumbered by the corrosion of the Al current collector, resulting in capacity loss and poor cycling stability. While ionic liquid electrolytes have been reported to suppress Al corrosion, a recent study found that pitting corrosion occurs even when ionic liquids are employed. This study investigates the effects of temperature and Na salt concentration on the Al corrosion behavior in different sulfonylamide-based ionic liquid electrolytes for sodium-ion batteries. In the present work, cyclic voltammetry measurements and scanning electron microscopy showed that severe Al corrosion occurred in ionic liquids at high temperatures and low salt concentrations. X-ray photoelectron spectroscopy was employed to identify the different elemental components and verify the thickness of the passivation layer formed under varied salt concentrations and temperatures. The differences in the corrosion behaviors observed under the various conditions are ascribed to the ratio of free $[FSA]^-$ anions to Na^+-coordinating $[FSA]^-$ in the electrolyte and the stability of the newly-formed passivation layer. This work aims at augmenting the understanding of Al corrosion behavior in ionic liquid electrolytes to develop advanced batteries.

Keywords: sodium-ion batteries, aluminum current collector, corrosion behavior, ionic liquid electrolyte, passivation layer

1. INTRODUCTION

Lithium-ion batteries (LIBs), accredited as the contemporary secondary batteries of choice, have gained dominant utility in portable electronic devices, electric vehicles, and energy storage systems (ESS).[1] Despite this widespread success, the increasing costs of lithium resources and the scarcity of critical elements such as Co and Ni present significant hurdles to the deployment of LIBs in large-scale ESS applications.[2, 3] These limitations have expedited the development of alternative battery technologies that utilize low-cost and earth-abundant materials. Among the secondary batteries fronted so far, sodium-ion batteries (SIBs) have emerged as promising candidates for grid-scale applications due to the environmental benignity and affordability of sodium resources.[4, 5] Besides the promise for improved feasibility, the progress of SIB development is further bolstered by the similarities in SIB and LIB intercalation chemistries which allow the appropriation of Na analogs of established LIB technologies.[6]

The success of SIBs as next-generation secondary batteries is highly contingent on the adoption of cheap, eco-friendly, and compatible battery components.[7-9] By this token, the lack of reactivity between Na metal and Al metal enables the utilization of Al foil as current collectors for both the negative and positive SIB electrodes, which presents significant cost benefits for these energy storage devices.[10-12] Besides economic viability, Al foil shows good electronic conductivity and mechanical durability.[13, 14] It is worth noting that even though the native Al_2O_3 passivation layer is formed on Al foil, Al current collectors are prone to attack and corrosion by sulfonylamide-based electrolytes during cycling at high potentials, leading to increased electrical resistance, electrolyte depletion, and capacity loss as well as poor cycling performance.[15-17] As such, comprehending Al corrosion behavior and exploring possible suppression measures is considered an essential requirement for next-generation SIBs.

Contemporary SIBs extensively utilize electrolytes containing organic carbonate solvents in combination with $NaPF_6$ or $NaClO_4$ salts due to their low viscosities and high ionic conductivities.[18, 19] Although Al current correctors are smoothly passivated in $NaPF_6$-based electrolytes, $NaPF_6$ is highly hygroscopic, which makes it prone to hydrolysis.[20-22] On the other hand, the explosive nature of $NaClO_4$ heavily hinders its application in electrolytes for safety reasons. In this light, sodium salts based on sulfonylamide anions, such as Na[FSA] ($[FSA]^-$ = bis(fluorosulfonyl)amide) and Na[TFSA] ($[TFSA]^-$ = bis(trifluoromethylsulfonyl)amide) are considered attractive options on the merits of their high stabilities, low toxicities, and safety.[23, 24] Compared to $NaPF_6$ and $NaClO_4$, sulfonylamide salts facilitate the formation of solid electrolyte interphase (SEI) with more inorganic species on the negative electrodes, enhancing the transport of Na ions and providing a more stable SEI layer.[25, 26] However, carbonate-based electrolytes employing Na[FSA] or Na[TFSA] salts tend to be corrosive towards the Al current collector at potentials above 4 V, thus deteriorating battery performance.[27-31]

Taking practical viability into account, organic electrolytes are considered unsuitable for high-temperature batteries because of their flammability and volatility.[32-34] In this context, ionic liquids (ILs) have attracted interest as alternative electrolytes on the grounds of their high thermal and electrochemical stability, negligible vapor pressure, low flammability, wide liquidus temperature range, and broad electrochemical window.[35-37] In fact, studies have shown that replacing organic electrolytes with ILs can be an effective strategy for accelerating the passivation of the Al surface.[38-47] Otaegui et al. compared the stability of the Al current collector in the propylene carbonate solution of Na[FSA] and ILs and revealed that the latter prevents Al corrosion at 55 °C up to 5 V (the former is 3.5 V).[48] Nevertheless, a recent study by our team revealed the occurrence of Al corrosion and severe capacity loss at elevated temperatures even after the

adoption of [FSA]-based IL electrolytes in SIBs.[49] In any case, the current understanding of the Al corrosion behavior in IL electrolytes containing Na[FSA] or Na[TFSA] remains relatively limited, providing the impetus for our inquest into the effects of these electrolytes on the Al current collector: specifically the influence of temperature and Na salt concentration. In particular, the effect of temperature on Al corrosion is an important point of interest, considering the possibilities of accidental heating[50, 51] or even the prospects of intermediate-temperature batteries exploiting the significant performance improvements embodied by IL electrolytes after temperature elevation.[36, 52, 53]

In this study, the effects of operating temperature and Na salt concentration on the corrosion behavior of the Al current collector are examined using [FSA]- and [TFSA]-based IL electrolytes formulated with two different ammonium cations: $[C_2C_1im]^+$ = 1-ethyl-3-methylimidazolium) and $[C_3C_1pyrr]^+$ = *N*-methyl-*N*-propylpyrrolidinium). The two cation species are typical for use in Li and Na ion batteries, according to previous works.[36] Herein, aluminum corrosion behavior is analyzed through a series of analyses based on cyclic voltammetry (CV), field emission scanning electron microscopy (FE-SEM), energy dispersive X-ray spectroscopy (EDX), Raman spectroscopy, X-ray fluorescence spectroscopy (XRF), and X-ray photoelectron spectroscopy (XPS).

2. EXPERIMENTAL SECTION

2.1 Materials and Electrolytes. The Na salts, Na[FSA] (Mitsubishi Materials Electronic Chemicals, purity > 99%) and Na[TFSA] (Kishida Chemical, purity > 99%), and organic salts, $[C_2C_1im][FSA]$, $[C_3C_1pyrr][FSA]$, $[C_2C_1im][TFSA]$, and $[C_3C_1pyrr][TFSA]$ (Kanto Chemical Co., Inc., purity > 99.9%), were dried under vacuum at 80 °C for 24 h before use. A series of IL

electrolytes with different Na^+ concentrations, as summarized in **Table S1**, were prepared by mixing the Na and organic salts in the target molar ratios in an argon-filled glove box (H_2O and O_2 < 1 ppm). The [TFSA] salt, $Al[TFSA]_3$, was synthesized using Al metal and bis(trifluoromethylsulfonyl)imide acid following procedures prescribed in a previous report.[54-56] Ethylene carbonate/dimethyl carbonate (EC/DMC = 1:1 v/v, battery grade, Kishida Chemical) was used without further purification. The organic electrolyte of 1 mol dm^{-3} Na[TFSA]-EC/DMC and 1 mol dm^{-3} Na[FSA]-EC/DMC were prepared by dissolving Na[FSA] or Na[TFSA] into EC/DMC.

2.2 Electrochemical Measurement. Coin cells (2032-type) used for CV measurements were assembled in the argon-filled glove box. Aluminum foil was punched into discs (diameter: 10 mm) and used as the working electrode. Metallic Na (spread into foil and pressed onto an Al plate) was used as the counter electrode (diameter: 13 mm). A glass fiber separator (Whatman, GF-A, diameter: 16 mm, and thickness: 260 μm) was used after immersion in the as-prepared electrolyte. CV measurements were performed using a VSP potentiostat (Bio-Logic) equipped with a thermostatic chamber (SU-242, ESPEC) at 25, 60, and 90 °C. CV was performed on the coin cells between 2 V and 6 V (vs. Na^+/Na) at a scan rate of 0.5 mV s^{-1} (the first cycle started from the rest potential).

2.3 Characterization and Analysis. After the CV tests, coin cells were disassembled, and the Al electrodes were rinsed with ethanol. The surface of Al electrodes (after ten cycles) was subjected to FE-SEM (Hitachi SU-8020) and EDX (Horiba EMAXEvolution X-max) analysis. The elemental composition of the surface of Al electrodes was analyzed by XPS (JEOL, JPS-9030, Mg Kα X-ray source). Depth profiles were obtained from the XPS data by etching Al electrodes using

an Ar beam with an accelerating voltage of 400 V. Raman spectra of the IL electrolytes were recorded by Raman spectroscopy (DXR3, Thermo Fisher Scientific) using a laser with a wavelength of 785 nm. For solubility tests of the $Al[TFSA]_3$ in different electrolytes, $Al[TFSA]_3$ was added to 1 mol dm^{-3} Na[TFSA]-EC/DMC, $Na_{0.1}[C_2C_1im]_{0.9}[TFSA]$, $Na_{0.2}[C_2C_1im]_{0.8}[TFSA]$, and $Na_{0.2}[C_3C_1pyrr]_{0.8}[TFSA]$ electrolytes. After these samples were stirred at 600 rpm at room temperature for one day, the content of Al species was determined by XRF spectroscopy (EDXL 300, Rigaku Corporation) under a He atmosphere.

3. RESULT AND DISCUSSION

In this study, the corrosion behavior of the Al current collector was analyzed by conducting CV measurements on Al electrodes in different sulfonylamide-based IL electrolytes at varied temperatures. **Figure 1** shows the CV curves of Al electrodes in a representative electrolyte: $Na_{0.2}[C_2C_1im]_{0.8}[FSA]$ IL measured at 25, 60, and 90 °C. Here, the anodic current is seen to gradually increase during the anodic scan and continues to rise even during the cathodic scan, achieving prominent peaks in the 4.4 to 6 V range. This anodic current is ascribed to electrolyte decomposition and Al corrosion during the electrochemical process.[13, 57] Markedly, the anodic current during the cathodic scan is larger than during the anodic scan, indicative of the exacerbated corrosion due to the increased electrode surface area after the removal of the native Al_2O_3 passivation film on the pristine Al foil and the dissolution of Al^{3+} species.[58, 59] The peak current density, approximately 0.02 mA cm^{-2} at 25 °C during the first cycle (**Figure 1a**), was observed to increase with temperature elevation and reached roughly six times higher at 90 °C (**Figure 1b, c**). The high current density evinces intensified Al electrode corrosion and severe electrolyte decomposition at elevated temperatures.[16] Even so, the anodic current was observed to decrease

with continued cycling, signaling the formation of a passivation layer. However, more CV scans are needed to passivate Al at elevated temperatures in contrast to 25 °C. Furthermore, it should be noted that if the passivation layer formed during the electrochemical measurement is not robust enough, the exposed part of the Al electrode will undergo further corrosion.[17] The stability of the passivation layer highly depends on the electrolyte composition and operation conditions, which will be also discussed below by combining with the CV results and XPS data.

For insight into their impact on Al corrosion, two sulfonylamide anion species ($[FSA]^-$ and $[TFSA]^-$) were employed in combination with two cation species ($[C_2C_1im]^+$ and $[C_3C_1pyrr]^+$) to prepare different IL electrolyte formulations with varied Na salt concentrations (see **Table S1** for the ILs used for this study and **Figures S1-S7** for CV curves in different concentrations and other IL electrolytes). For the $Na_x[C_2C_1im]_{1-x}[FSA]$ electrolytes, the anodic current was noted to decrease with increasing Na^+ fraction, providing negligible anodic current for the $Na_{0.5}[C_2C_1im]_{0.5}[FSA]$ electrolyte at 25 °C (**Figures S2** and **S3**). The CV curves obtained from the $Na_x[C_3C_1pyrr]_{1-x}[FSA]$ electrolytes exhibited similar effects of temperature and Na^+ concentration on the anodic current, although their current densities were generally lower than the $Na_x[C_2C_1im]_{1-x}[FSA]$ electrolytes (**Figures S5-S7**). In addition, the CV curves obtained from the $Na_{0.2}[C_2C_1im]_{0.8}[TFSA]$ electrolyte reveal that temperature elevation engendered significant increases in the anodic current, as shown in **Figure S1**. The highest anodic current of $Na_{0.2}[C_3C_1pyrr]_{0.8}[TFSA]$ electrolyte was observed at 60 °C. Notably, the anodic current for $Na_{0.2}[C_3C_1pyrr]_{0.8}[TFSA]$ electrolyte at 90 °C was observed to be an order of magnitude lower than that of the $Na_{0.2}[C_2C_1im]_{0.8}[TFSA]$ electrolyte at the same temperature (**Figure S4**). The effect of cations on different CV curves will be discussed below.

Figures 2 and **S8** summarize the total charge calculated by integrating the total anodic peak

area of the cyclic voltammogram of each cycle (**Figure 2** for the $[C_2C_1im]$-based ILs and **Figure S8** for the $[C_3C_1pyrr]$-based ILs). The total charge exhibits a clear correlation to the Na^+ concentration in the $Na_x[C_2C_1im]_{1-x}[FSA]$ IL electrolyte and the operating temperatures (**Figure 2)**. When the temperature is kept constant, increasing the Na^+ fraction of the electrolyte results in a continuous decrease in the total charge. On the other hand, temperature elevation is noted to engender an increase in the total charge during the initial few cycles. Notably, the total charge of the $Na_{0.2}[C_2C_1im]_{0.8}[TFSA]$ electrolyte is less than the $Na_{0.2}[C_2C_1im]_{0.8}[FSA]$ electrolyte at 25 °C. However, these trends are inversed at elevated temperatures; the $Na_{0.2}[C_2C_1im]_{0.8}[TFSA]$ electrolyte exhibits larger total charge values, which do not significantly decrease even with repeated CV scans. These results suggest that the passivation process in the $Na_{0.2}[C_2C_1im]_{0.8}[TFSA]$ electrolyte fails at 60 and 90 °C, resulting in severe Al corrosion.

The total charge data obtained from the $[C_3C_1pyrr]$-based IL electrolytes betoken similar trends as illustrated in **Figure S8**. However, the total charge values derived from the $[C_3C_1pyrr]$-based electrolytes are found to be significantly lower than those from the $[C_2C_1im]$-based electrolytes. Further, temperature elevation of the $[C_3C_1pyrr]$-based electrolytes is seen to have less effect on the resultant total charge than in the case of the $[C_2C_1im]$-based electrolytes. Here, the total charge values at 60 °C are higher than at 90 °C, which may attribute to the dissolution and reconstruction of the unstable passivation layer formed at 60 °C. These observations indicate that the Al corrosion behavior in the $[C_3C_1pyrr]$-based electrolytes is intrinsically different from the one in the $[C_2C_1im]$-based electrolytes. The passivation layer formed based on the $[C_3C_1pyrr]$-based electrolytes might contain beneficial components to slow down the side reaction and facilitate Al passivation contrast to the $[C_2C_1im]$-based electrolytes. Another possible reason for such differences is the higher anodic stability of the $[C_3C_1pyrr]^+$ compared to that of the $[C_2C_1im]^+$

cations.[60] Besides, differences in Al corrosion behavior could also be rationalized by the differences in the ratios of the free $[FSA]^-$ (non-coordinating to Na^+, abbreviated as FR) to coordinating $[FSA]^-$ (coordinating to Na^+, abbreviated as CDN) in the ILs. The coordination states of $[FSA]^-$ in ILs can easily be determined through Raman spectrometry, where the S-N-S bending mode shifts, depending on the coordination state to Na^+ (~730 cm^{-1} for FR $[FSA]^-$ and above 740 cm^{-1} for CDN $[FSA]^-$).[61] When the two states of $[FSA]^-$, CDN and FR, are assumed, the ratio of CDN/FR is higher for the $[C_3C_1pyrr]$-based electrolyte (50/50) than for the $[C_2C_1im]$-based electrolyte (36/64) (**Figure S9**). Consequently, $[FSA]^-$ is more electron deficient and more resistive to oxidation in the $[C_3C_1pyrr]$-based electrolyte (see the discussion of the Raman spectroscopy below for details).

For the aim of understanding the corrosion process of Al foil, further discussion will be made for the $Na_x[C_2C_1im]_{1-x}[FSA]$ electrolytes that exhibit the representative characteristics in the following. Additional results from the other ILs are included in Supporting Information.

The surface morphology and elemental composition of the Al electrode surface after CV measurements were subsequently evaluated using FE-SEM and EDX techniques to visually confirm Al corrosion behavior. **Figure 3** shows the FE-SEM and EDX mapping images of Al electrodes cycled in the $Na_{0.2}[C_2C_1im]_{0.8}[FSA]$ electrolyte under different operating temperatures. **Figure 4** shows the corresponding electrodes cycled in varied Na^+ concentrations using a series of $Na_x[C_2C_1im]_{1-x}[FSA]$ electrolytes, respectively (see **Figure S10-S16** for FE-SEM and EDX mapping images related to other conditions and electrolytes). As illustrated, the surfaces of the Al electrodes cycled in $Na_{0.2}[C_2C_1im]_{0.8}[FSA]$ reveal typical pitting corrosion in the range of temperatures investigated. At 25 °C, corrosion pits with diameters of < 50 μm are observed on the entire electrode surfaces (**Figure 3**). Additionally, the corrosion pits are noted to become larger

with increasing temperature, eventually becoming interconnected at 90 °C due to severe corrosion. The EDX mapping images show the presence of Al, F, S, O, N, and Na elements on the electrode surfaces. The images also show an even distribution of F, S, and O elements in the corrosion pits, suggesting that $[FSA]^-$ is deeply involved in the corrosion process. On an interesting note, Al was hardly detected in the corrosion pits. These results evince that $[FSA]^-$ reacts with the native oxide on the Al current collector, and the Al^{3+} reacts with the amide anions to form complexes that are dissolved into the electrolyte as has been previously proposed in studies on organic solvent electrolytes.[18, 27]

The correlation between the Na^+ concentration and Al corrosion behavior at 25 °C is demonstrated in **Figure 4**. Here, the FE-SEM images illustrate numerous pits on the surface of the Al electrode cycled in the $Na_{0.2}[C_2C_1im]_{0.8}[FSA]$ electrolyte. In contrast, only a few pits are observed on the Al electrode cycled in the $Na_{0.3}[C_2C_1im]_{0.7}[FSA]$ electrolyte. The diameters of the corrosion pits are found to decrease with increasing Na^+ fractions: an affirmation that increasing the Na^+ concentration can suppress corrosion of the Al electrode. Furthermore, the pitting corrosion is not seen on the electrodes obtained from the $Na_{0.5}[C_2C_1im]_{0.5}[FSA]$ electrolyte at 25 °C, in congruence with the negligible anodic current visualized in the CV curves (**Figure S3a**). These observations are consistent with the CV results wherein the anodic current significantly decreases when the Na salt fraction is increased (**Figures S2** and **S3**). Likewise, the $[C_3C_1pyrr]$-based electrolytes exhibited similar Al corrosion behavior when subjected to analogous operating temperatures and Na salt concentrations (**Figures S13-16)**.

It is worth noting that hemispherical deposits appeared on the surface of the Al electrode when the Na salt concentration was increased. These deposits are presumed to be a new passivation layer formed by the decomposition of the IL electrolytes (**Figures 4b and c**). These hemispherical

deposits were also found on the Al electrode after CV measurements were performed in the $Na_{0.2}[C_2C_1im]_{0.8}[TFSA]$ and $Na_{0.2}[C_3C_1pyrr]_{0.8}[TFSA]$ IL electrolytes (**Figures S10 and S13**, respectively). The results suggest that the degree of Al corrosion is highly contingent on the properties of the passivation layer formed during the electrochemical process. Notably, the [TFSA]-based ILs manifested slightly better passivation capabilities at 25 °C than [FSA]-based ILs. However, these capabilities were seen to drastically diminish at elevated temperatures in the case of the $Na_{0.2}[C_2C_1im]_{0.8}[TFSA]$ IL electrolyte.

In previous studies by Kühnel et al. and Garcia et al., the Al complex formed during the corrosion process was found to have considerably lower solubility in IL electrolytes than the ones in organic carbonate-based electrolytes, and thus ILs facilitate the formation of a more effective passivation layer that resists Al corrosion.[40, 62] Since Al corrosion is not so severe in the IL electrolytes at high Na^+ fractions in this work, it is reasonable to tentatively postulate that the solubility of Al complexes into electrolytes is a major reason for the different corrosion behaviors observed. As such, $Al[TFSA]_3$, whose synthesis route has been established in previous works, was subjected to solubility measurements involving the various electrolytes in the present work (preparation of $Al[FSA]_n^{(3-n)+}$ complex is not well-established). According to XRF analysis (**Table S2**), the solubility of $Al[TFSA]_3$ into 1 mol dm^{-3} Na[TFSA]-EC/DMC is noted to be approximately two times higher than in the ILs. Even so, the difference between the organic electrolyte and the IL is insignificant, considering their vastly different Al corrosion behaviors (**Figure S17**). Moreover, the differences in the Al concentrations of the ILs are subtle which demonstrate that the solubility of the Al complexes is not the main reason for the different Al corrosion behaviors.

The factors influencing the Al corrosion behavior can also be postulated to involve both the operating temperatures and Na salt concentrations. In this conjecture, the passivation layers formed

on Al electrodes cycled at lower temperatures and high concentration conditions are considered more robust or better stabilized than those formed at higher temperatures and low Na^+ concentration conditions. As such, the passivation layer formed during cycling was subjected to stability tests through further CV analysis to verify this hypothesis. First, ten consecutive CV cycles were performed without intervals to sufficiently form a passivation layer. Subsequently, five CV cycles were performed with an interval (12-hour rest) after each cycle (**Figure S18**). This interval was set to determine the stability of the newly-formed passivation layer. Specifically, if the passivation layer dissolves during an interval, extra capacity is required to reform the passivation layer during the next cycle. **Figures 5a and 5b** summarize the total charge during the 10th, 12th, and 14th anodic scans of CV in the $Na_x[C_2C_1im]_{1-x}[FSA]$ electrolytes (x = 0.2 and 0.5) at 25 °C (**Figure 5a**) and 90 °C (**Figure 5b**). When x = 0.2, the total charge at 90 °C increases at the subsequent 14th cycle, whereas it remains relatively stable at 25 °C. Correspondingly, the current density decreases at the 12th cycle but increases at the 14th cycle (**Figure S18c**), suggesting that the passivation layer dissolves and Al corrosion and electrolyte decomposition occur again if intervals are taken after each cycle. In the case of x = 0.5, the total charge was lower than that of x = 0.2 during measurements performed at 25 °C and 90 °C. This observation suggests that less charge participates in the repetitive passivation process, and the passivation layer remains stable during the cycles with intervals.

XPS analyses were performed to elucidate the chemical composition of the passivation layer formed on the Al electrode after the first cycle of the CV measurements under different temperature and concentration conditions. As shown in **Figure 5c**, the F 1s XPS spectra for Al electrodes were deconvoluted into three different contributions.[44, 63, 64] The peak at 686.6 eV is assigned to the F atom involved in an ionic bond such as Al−F. The presence of $-SO_xF$ is identified

by the peaks at 688.0 and 689.4 eV. Comparing the passivation layers formed by each electrolyte at different temperatures shows the ratio of -SO_xF to Al−F at 90 °C is higher than that of 25 °C, evincing that the passivation layer formed at 90 °C has more components derived from $[FSA]^-$ decomposition. XPS depth profiles (**Figure 5d**) were also obtained to illustrate the relative thickness of the passivation layer on the surface of the Al current collectors. Here, the F 1s peak intensities of the electrodes cycled at 90 °C exhibit a more gradual decrease with increasing etching time compared to those measured for the electrodes cycled at 25 °C: an indicator that cycling at 90 °C forms a thicker passivation layer. This observation is in accord with the XPS results of Al 2p (**Figure S19**), where the peak intensity of Al metal on electrodes cycled at 90 °C increases more gently with increasing etching time than those cycled at 25 °C: evidence that the thicker passivation layer covers the Al substrate at 90 °C.

The difference in ion-ion interactions in the electrolytes with respect to Na salt concentration was studied by Raman spectroscopy to clarify the effects of the electrolyte structure on the Al corrosion behavior. **Figure S20** presents the Raman spectra of the FSA-based IL electrolytes at various Na[FSA] concentrations (see **Figure S21** for [TFSA]-based ILs). The peaks in the region between 700 and 800 cm^{-1} are assigned to the S-N-S bending mode, which can be deconvoluted to those of free $[FSA]^-$ and Na^+-coordinating $[FSA]^-$ as mentioned in the discussion above (FR and CDN, respectively).[65] The peak in this region exhibits a blue shift with increasing Na salt concentration regardless of the cationic species, suggesting an increase of the CDN $[FSA]^-$ and a decrease of the FR $[FSA]^-$. This phenomenon may affect the Al corrosion behavior in two distinct ways: the formation of passivation layers with different thicknesses and the reaction for the dissolution of the native Al_2O_3 passivation layer. The increase of CDN $[FSA]^-$ can lead to the formation of a thinner passivation layer because CDN $[FSA]^-$ is more electron deficient and

oxidatively robust than FR $[FSA]^-$.[66] Consequently, the thinner passivation layer sufficiently prevents further reactions caused by the contact between the electrode surface and the electrolyte with oxidatively robust anions. On the other hand, FR $[FSA]^-$ is more reactive to Al_2O_3 because it has more coordinating ability than CDN $[FSA]^-$.[67-70]

Based on the results above, the possible mechanism of Al corrosion behavior is illustrated in **Figure 6**. Here two of the most severe and the mildest conditions of high Na^+ concentration and low temperature (Figure 6a) and low Na^+ concentration and high temperature (Figure 6b) are selected to visualize and simplified the mechanism. As shown in the schematic, free [FSA] anions are adsorbed on the native Al_2O_3 passivation film, which decays the film at high potentials along with O_2 generation and Al^{3+} dissolution in the form of $Al[anion]_n^{(3-n)+}$. As Raman spectra clearly indicate a blue shift of peaks with increasing Na salt concentration, which explains the severer corrosion degree of the native Al_2O_3 passivation film at the initial cycle at low Na^+ concentration and high temperature condition by free [FSA] anions. It is because electrolytes with low Na^+ concentrations have more free $[FSA]^-$ anions that vigorously abrade the native Al_2O_3 passivation layer and accelerate the corrosion process. Moreover, the newly-formed passivation layer is less stable and is dissolved during cycling at low Na^+ concentration and high temperature condition. Markedly, the passivation layer is seen to dissolve progressively at elevated temperatures, especially with electrolytes of lower Na salt concentrations. Whereas under high Na^+ concentration and low temperature conditions, the ratio of free [FSA] anions to Na^+-coordinating $[FSA]^-$ is low, forming a new passivation layer with very low solubility in the electrolytes. As discussed in **Figure 5(a)**, this passivation layer keeps robust to protect the Al electrode. Accordingly, a thicker passivation layer formed by the decomposition of the electrolyte is required to comprehensively cover the Al electrode surface. Otherwise, Al corrosion occurred again after the breakdown of the

passivation layer. Veritably, increasing the Na salt concentration of the electrolytes suppresses the Al corrosion process to a certain extent but does not alleviate severe Al corrosion when temperatures are elevated.

4. CONCLUSION

In summary, the present study explores the effects of temperature and salt concentration variations on the corrosion behavior of the Al current collector in IL electrolytes. CV results showed that the anodic current increases with increasing temperature and decreasing Na^+ concentrations. SEM images after CV measurements revealed that Al corrosion was exacerbated in electrolytes with low Na^+ concentration and suppressed for electrolytes with high Na^+ concentration at room temperature. Even so, the electrolytes with high Na^+ concentration were still ineffective in suppressing Al corrosion at elevated temperatures. EDX mapping further revealed the involvement of $[FSA]^-$ anions in the Al corrosion. XRF measurements confirmed that the solubility of Al complexes in the electrolytes investigated is not the primary cause of the different corrosion degrees observed. The results from the present analyses suggest that the differences in Al corrosion behavior are caused by the variegated stabilities of the newly-formed passivation layers on the surfaces. The Al corrosion process in electrolytes with high Na^+ concentrations is possibly alleviated by the more robust passivation layer formed with Na^+-coordinating $[FSA]^-$. However, this robust passivation layer becomes unstable when the temperature is elevated, consuming extra capacity to form a new passivation layer at every cycle. The results presented herein promise to augment the present understanding of the corrosion behavior of Al current collectors in a range of ILs electrolytes. Accordingly, future inquests into the surface modification of Al current collectors

can be expected to be a propitious strategy for enhancing the performance of SIBs using IL electrolytes.

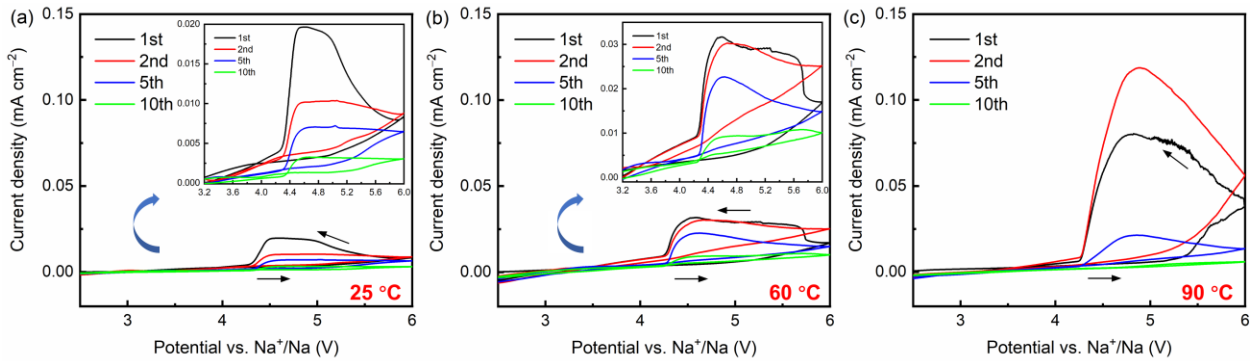

Figure 1. Cyclic voltammograms of an Al electrode in the $Na_{0.2}[C_2C_1im]_{0.8}[FSA]$ IL electrolyte at (a) 25, (b) 60, and (c) 90 °C from the rest potential to 6 V. Scan rate: 0.5 mV s^{-1}. The black arrows indicate the scan direction. The insets show the enlarged part of the cyclic voltammograms (see **Figures S1-S7** in the Supporting Information for cyclic voltammograms in other concentrations and other IL electrolytes and see **Figure 2** for the summary of total charges during anodic scans of CV results for the Al electrodes in different electrolytes.)

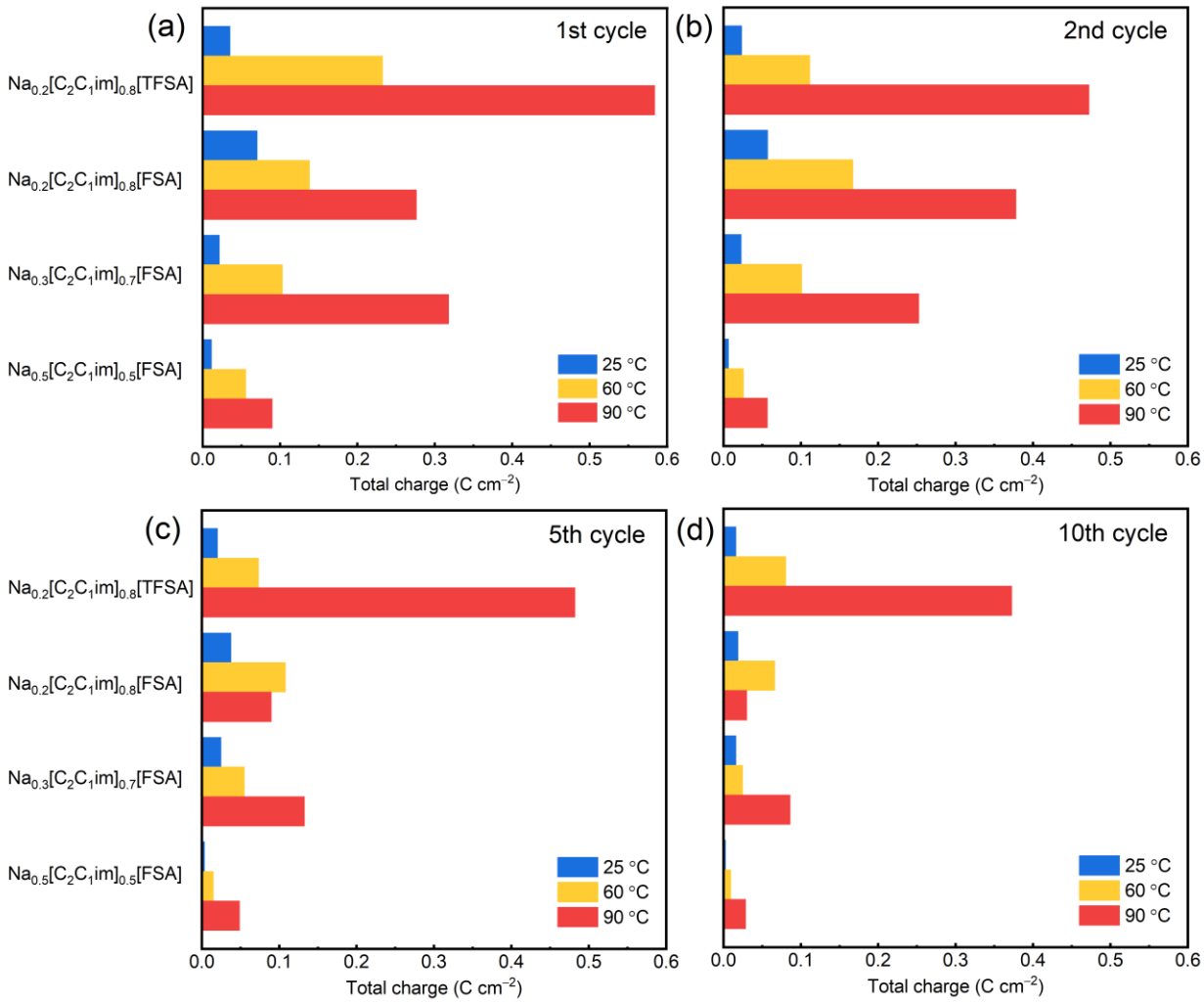

Figure 2. Summary of total charges during anodic scans in the CV measurements in the $[C_2C_1im]$-based IL electrolytes at the (a) 1st, (b) 2nd, (c) 5th, and (d) 10th cycles (see **Figures 1** and **S1-S3** for the corresponding cyclic voltammograms). Temperature: 25, 60, and 90 °C. The total charges were calculated by integrating the anodic current. **Figure S8** summarizes total charges during anodic scans in the CV measurements in the $[C_3C_1pyrr]$-based IL electrolytes corresponding to the CV curves in **Figures S4-S7**.

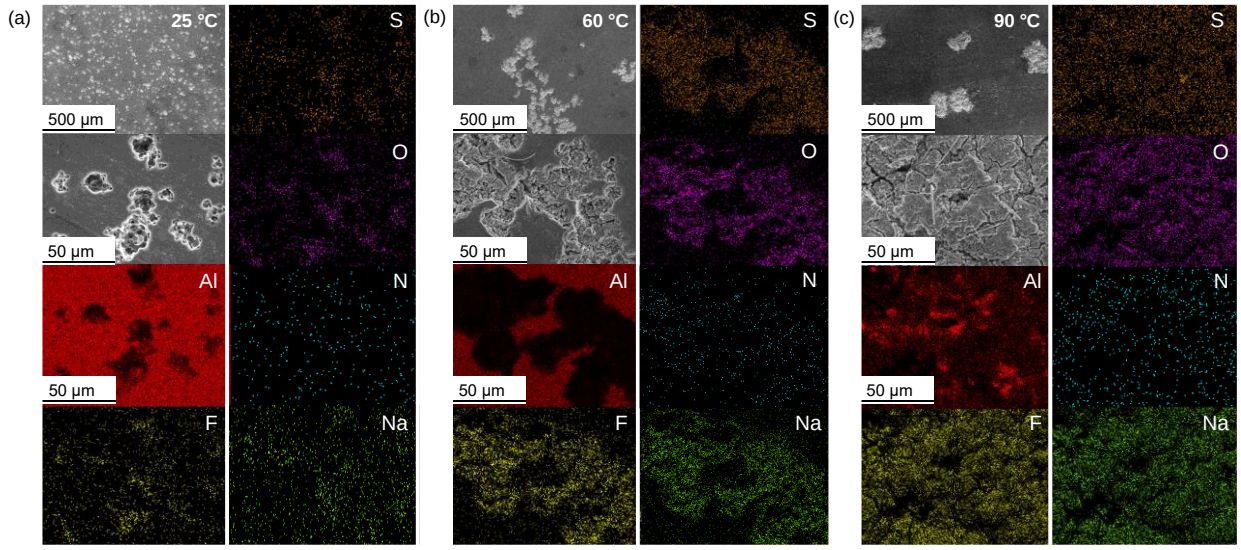

Figure 3. Temperature dependence of FE-SEM and EDX mapping images for the Al electrode after the 10 cycles of CV measurements in the $Na_{0.2}[C_2C_1im]_{0.8}[FSA]$ electrolyte at (a) 25, (b) 60, and (c) 90 °C.

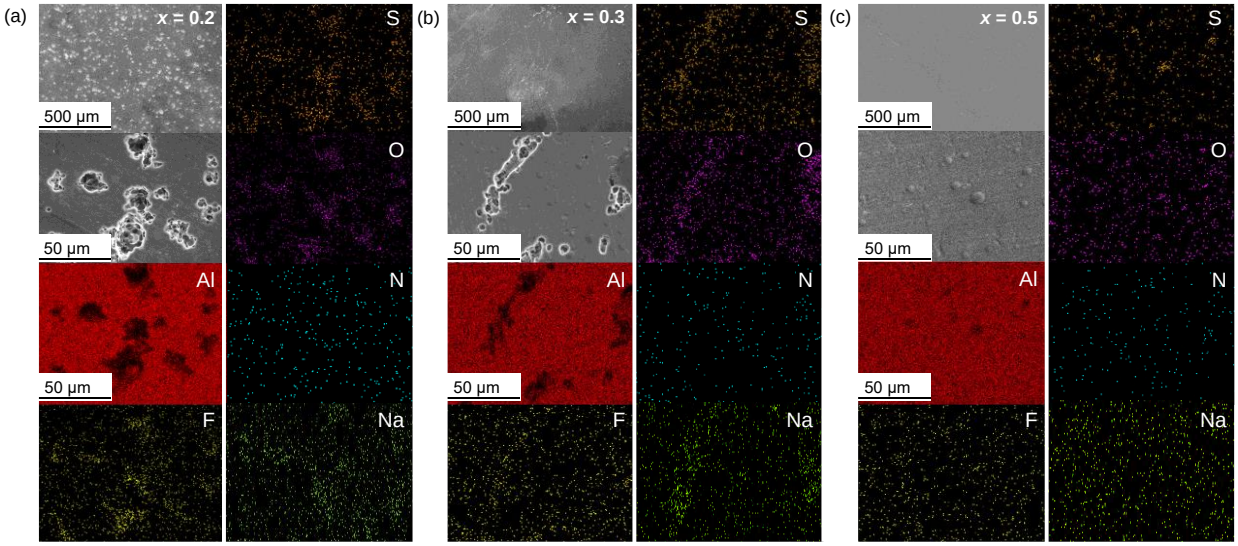

Figure 4. Na salt fraction dependence of FE-SEM and EDX mapping images for the Al electrode after the 10 cycles of CV measurements at 25 °C in the $Na_x[C_2C_1im]_{1-x}[FSA]$ electrolyte, (a) x = 0.2, (b) x = 0.3, and (c) x = 0.5, respectively. (**Figure 4(a)** is the same as **Figure 3(a)**, added once again here for comparison.)

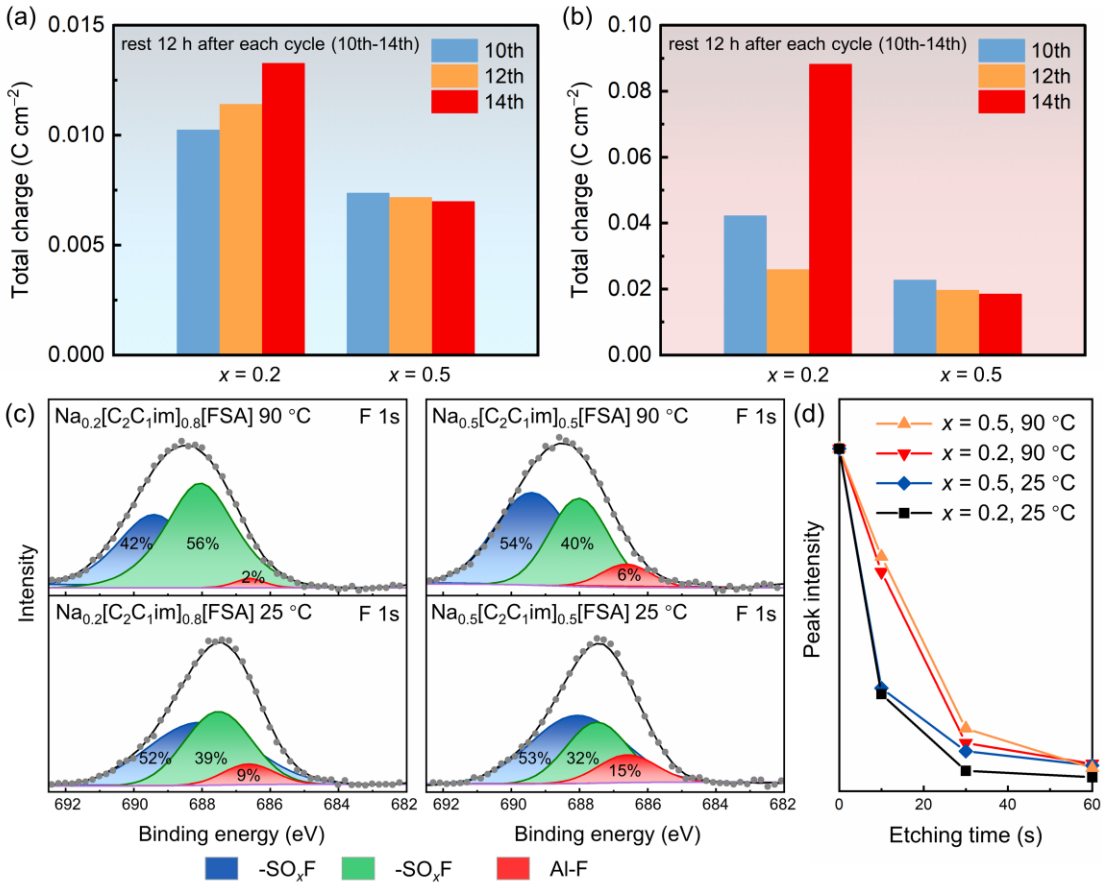

Figure 5. (a, b) Comparison of total charges during anodic scans of the CV measurements at (a) 25 °C and (b) 90 °C. (c) F 1s XPS spectra of the Al electrodes after the first cycle of the CV measurements at 25 °C and 90 °C. Electrolyte: $Na_x[C_2C_1im]_{1-x}[FSA]$ ILs (x = 0.2 and 0.5). (d) Depth profile of F atom on the Al electrode before and after the first cycle of the CV measurements at 25 °C and 90 °C based on the F 1s XPS peak intensity against etching time.

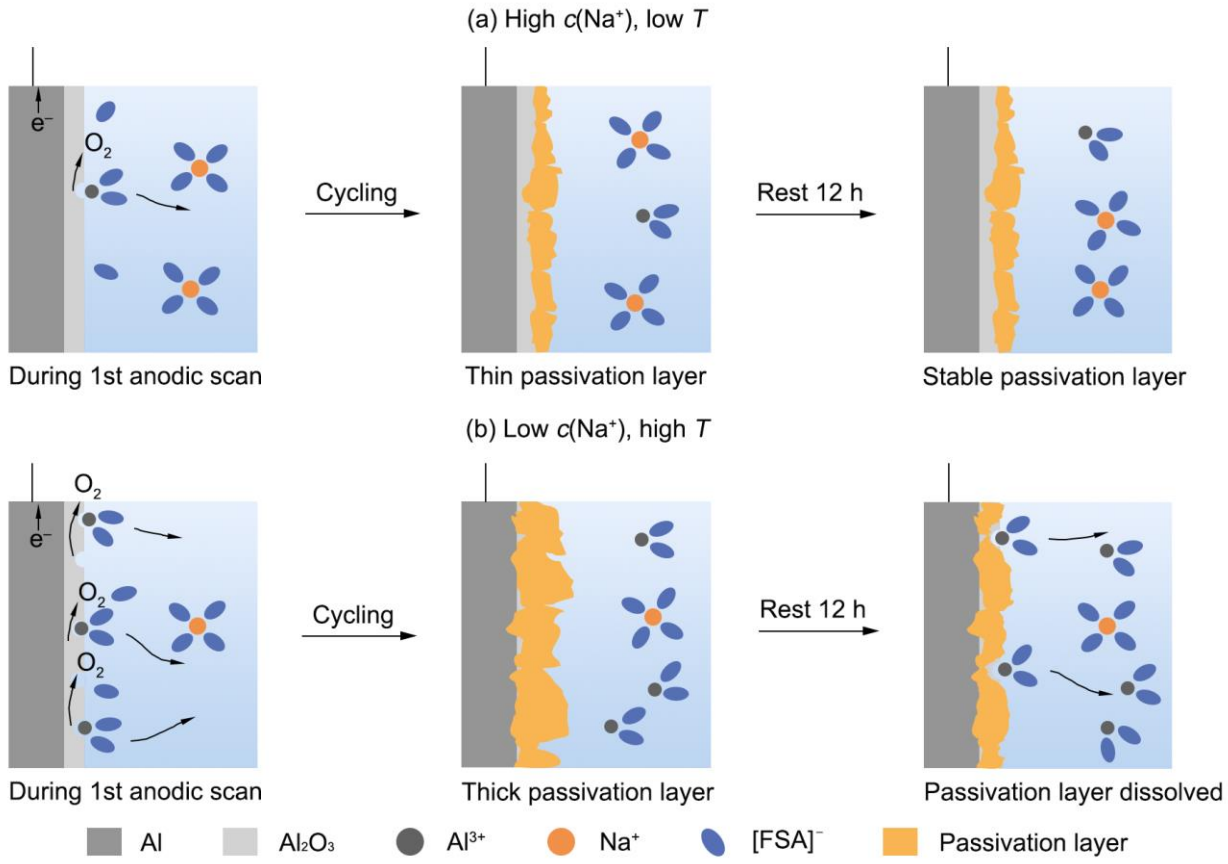

Figure 6. Schematic illustration of the formation and dissolution processes for the passivation layer on the Al electrodes in the investigated IL electrolytes (a) under high Na^+ concentration and low temperature conditions and (b) under low Na^+ concentration and high temperature conditions.

ASSOCIATED CONTENT

Supporting Information.

The Supporting Information is available free of charge at DOI: xx.

Additional experimental results of cyclic voltammograms in other IL electrolytes, SEM and EDX mapping images, Raman spectra, XRF results, and XPS data with peak assignments (PDF)

AUTHOR INFORMATION

Corresponding Author

*Phone: +81 75 753 5827. Fax: +81 75 753 5906. E-mail: k-matsumoto@energy.kyoto-u.ac.jp (K.M.). hwang.jinkwang.5c@kyoto-u.ac.jp (J.H)

ORCID

Huazhen Liu: 0000-0001-6745-9885

Jinkwang Hwang: 0000-0003-4800-3158

Kazuhiko Matsumoto: 0000-0002-0770-9210

Rika Hagiwara: 0000-0002-7234-3980

Notes

The authors declare no competing financial interest.

ACKNOWLEDGMENT

This study was supported by Grant-in-Aid for Scientific Research(B) conducted through the support of the Grant number 21H02047.

REFERENCES

(1) Hannan, M. A.; Lipu, M. H.; Hussain, A.; Mohamed, A. A Review of Lithium-Ion Battery State of Charge Estimation and Management System in Electric Vehicle Applications: Challenges and Recommendations. *Renew. Sust. Energ. Rev.* **2017**, *78*, 834-854.

(2) Yabuuchi, N.; Kubota, K.; Dahbi, M.; Komaba, S. Research Development on Sodium-Ion Batteries. *Chem. Rev.* **2014**, *114*, 11636-11682.

(3) Hirsh, H. S.; Li, Y.; Tan, D. H. S.; Zhang, M.; Zhao, E.; Meng, Y. S. Sodium-Ion Batteries Paving the Way for Grid Energy Storage. *Adv. Energy Mater.* **2020**, *10*, 2001274.

(4) Dunn, B.; Kamath, H.; Tarascon, J.-M. Electrical Energy Storage for the Grid: A Battery of Choices. *Science* **2011**, *334*, 928-935.

(5) Niu, Y.; Zhao, Y.; Xu, M. Manganese-Based Polyanionic Cathodes for Sodium-Ion Batteries. *Carbon Neutralization* **2023**, *2*, 150-168.

(6) Du, P.; Cao, L.; Zhang, B.; Wang, C.; Xiao, Z.; Zhang, J.; Wang, D.; Ou, X. Recent Progress on Heterostructure Materials for Next-Generation Sodium/Potassium Ion Batteries. *Renew. Sust. Energ. Rev.* **2021**, *151*, 111640.

(7) Larcher, D.; Tarascon, J. M. Towards Greener and More Sustainable Batteries for Electrical Energy Storage. *Nat. Chem.* **2015**, *7*, 19-29.

(8) Wang, K.; Wang, C.; Yang, H.; Wang, X.; Cao, F.; Wu, Q.; Peng, H. Vertical Graphene Nanosheetsmodified Al Current Collectors for High-Performance Sodium-Ion Batteries. *Nano Res.* **2020**, *13*, 1948-1954.

(9) Casas, X.; Niederberger, M.; Lizundia, E. A Sodium-Ion Battery Separator with Reversible Voltage Response Based on Water-Soluble Cellulose Derivatives. *ACS Appl. Mater. Interfaces* **2020**, *12*, 29264-29274.

(10) Murray, J. L. The Al−Na (Aluminum-Sodium) System. *Bull. Alloy Phase Diagr.* **1983**, *4*, 407-410.

(11) Kundu, D.; Talaie, E.; Duffort, V.; Nazar, L. F. The Emerging Chemistry of Sodium Ion Batteries for Electrochemical Energy Storage. *Angew. Chem. Int. Ed.* **2015**, *54*, 3431-3448.

(12) Vaalma, C.; Buchholz, D.; Weil, M.; Passerini, S. A Cost and Resource Analysis of Sodium-Ion Batteries. *Nat. Rev. Mater.* **2018**, *3*, 18013.

(13) Zhang, S. S.; Jow, T. R. Aluminum Corrosion in Electrolyte of Li-Ion Battery. *J. Power Sources* **2002**, *109*, 458-464.

(14) Huang, Y.; Zhao, L.; Li, L.; Xie, M.; Wu, F.; Chen, R. Electrolytes and Electrolyte/Electrode Interfaces in Sodium-Ion Batteries: From Scientific Research to Practical Application. *Adv. Mater.* **2019**, *31*, 1808393.

(15) Braithwaite, J. W.; Gonzales, A.; Nagasubramanian, G.; Lucero, S. J.; Peebles, D. E.; Ohlhausen, J. A.; Cieslak, W. R. Corrosion of Lithium-Ion Battery Current Collectors. *J. Electrochem. Soc.* **1999**, *146*, 448-456.

(16) Li, X.; Deng, S.; Banis, M. N.; Doyle-Davis, K.; Zhang, D.; Zhang, T.; Yang, J.; Divigalpitiya, R.; Brandys, F.; Li, R.; Sun, X. Suppressing Corrosion of Aluminum Foils Via Highly Conductive Graphene-Like Carbon Coating in High-Performance Lithium-Based Batteries. *ACS Appl. Mater. Interfaces* **2019**, *11*, 32826-32832.

(17) Chen, J.; Bai, Z.; Li, X.; Wang, Q.; Du, J.; Lu, R.; Liu, X. Reduced Graphene Oxide-Modified Aluminum Foils as Highly Conductive and Corrosion-Resistant Cathode Current Collectors for Li-Ion Batteries. *Appl. Surf. Sci.* **2022**, *606*, 155002.

(18) Eshetu, G. G.; Grugeon, S.; Kim, H.; Jeong, S.; Wu, L.; Gachot, G.; Laruelle, S.; Armand, M.; Passerini, S. Comprehensive Insights into the Reactivity of Electrolytes Based on Sodium Ions. *ChemSusChem* **2016**, *9*, 462-471.

(19) Zheng, X.; Gu, Z.; Liu, X.; Wang, Z.; Wen, J.; Wu, X.; Luo, W.; Huang, Y. Bridging the Immiscibility of an All-Fluoride Fire Extinguishant with Highly-Fluorinated Electrolytes toward Safe Sodium Metal Batteries. *Energ. Environ. Sci.* **2020**, *13*, 1788-1798.

(20) Ponrouch, A.; Marchante, E.; Courty, M.; Tarascon, J.-M.; Palacin, M. R. In Search of an Optimized Electrolyte for Na-Ion Batteries. *Energ. Environ. Sci.* **2012**, *5*, 8572-8583.

(21) Dahbi, M.; Nakano, T.; Yabuuchi, N.; Fujimura, S.; Chihara, K.; Kubota, K.; Son, J.-Y.; Cui, Y.-T.; Oji, H.; Komaba, S. Effect of Hexafluorophosphate and Fluoroethylene Carbonate on Electrochemical Performance and the Surface Layer of Hard Carbon for Sodium-Ion Batteries. *ChemElectroChem* **2016**, *3*, 1856-1867.

(22) Barnes, P.; Smith, K.; Parrish, R.; Jones, C.; Skinner, P.; Storch, E.; White, Q.; Deng, C.; Karsann, D.; Lau, M. L.; Dumais, J. J.; Dufek, E. J.; Xiong, H. A Non-Aqueous Sodium Hexafluorophosphate-Based Electrolyte Degradation Study: Formation and Mitigation of Hydrofluoric Acid. *J. Power Sources* **2020**, *447*, 227363.

(23) Zhao, L.; Zhao, J.; Hu, Y.-S.; Li, H.; Zhou, Z.; Armand, M.; Chen, L. Disodium Terephthalate (Na2c8h4o4) as High Performance Anode Material for Low-Cost Room-Temperature Sodium-Ion Battery. *Adv. Energy Mater.* **2012**, *2*, 962-965.

(24) Ould, D. M.; Menkin, S.; Smith, H. E.; Riesgo-Gonzalez, V.; Jónsson, E.; O'Keefe, C. A.; Coowar, F.; Barker, J.; Bond, A. D.; Grey, C. P. Sodium Borates: Expanding the Electrolyte Selection for Sodium-Ion Batteries. *Angew. Chem.* **2022**, e202202133.

(25) Eshetu, G. G.; Diemant, T.; Hekmatfar, M.; Grugeon, S.; Behm, R. J.; Laruelle, S.; Armand, M.; Passerini, S. Impact of the Electrolyte Salt Anion on the Solid Electrolyte Interphase Formation in Sodium Ion Batteries. *Nano Energy* **2019**, *55*, 327-340.

(26) Ding, Y.; Guo, X.; Qian, Y.; Gao, H.; Weber, D. H.; Zhang, L.; Goodenough, J. B.; Yu, G. In Situ Formation of Liquid Metals Via Galvanic Replacement Reaction to Build Dendrite-Free Alkali-Metal-Ion Batteries. *Angew. Chem. Int. Ed.* **2020**, *59*, 12170-12177.

(27) Yang, H.; Kwon, K.; Devine, T. M.; Evans, J. W. Aluminum Corrosion in Lithium Batteries an Investigation Using the Electrochemical Quartz Crystal Microbalance. *J. Electrochem. Soc.* **2000**, *147*, 4399.

(28) Hatchard, T.; Obrovac, M. Evaluation of Electrolyte Salts and Solvents for Na-Ion Batteries in Symmetric Cells. *J. Electrochem. Soc.* **2014**, *161*, A1748.

(29) Park, K.; Yu, S.; Lee, C.; Lee, H. Comparative Study on Lithium Borates as Corrosion Inhibitors of Aluminum Current Collector in Lithium Bis(Fluorosulfonyl)Imide Electrolytes. *J. Power Sources* **2015**, *296*, 197-203.

(30) Lee, J.; Lee, Y.; Lee, J.; Lee, S.-M.; Choi, J.-H.; Kim, H.; Kwon, M.-S.; Kang, K.; Lee, K. T.; Choi, N.-S. Ultraconcentrated Sodium Bis(Fluorosulfonyl)Imide-Based Electrolytes for High-Performance Sodium Metal Batteries. *ACS Appl. Mater. Interfaces* **2017**, *9*, 3723-3732.

(31) Geng, C.; Buchholz, D.; Kim, G.-T.; Carvalho, D. V.; Zhang, H.; Chagas, L. G.; Passerini, S. Influence of Salt Concentration on the Properties of Sodium-Based Electrolytes. *Small Methods* **2019**, *3*, 1800208.

(32) Zeng, Z.; Jiang, X.; Li, R.; Yuan, D.; Ai, X.; Yang, H.; Cao, Y. A Safer Sodium-Ion Battery Based on Nonflammable Organic Phosphate Electrolyte. *Adv. Sci.* **2016**, *3*, 1600066.

(33) Che, H.; Chen, S.; Xie, Y.; Wang, H.; Amine, K.; Liao, X.-Z.; Ma, Z.-F. Electrolyte Design Strategies and Research Progress for Room-Temperature Sodium-Ion Batteries. *Energ. Environ. Sci.* **2017**, *10*, 1075-1101.

(34) Sun, Y.; Shi, P.; Xiang, H.; Liang, X.; Yu, Y. High-Safety Nonaqueous Electrolytes and Interphases for Sodium-Ion Batteries. *Small* **2019**, *15*, 1805479.

(35) Wasserscheid, P.; Keim, W. Ionic Liquids—New "Solutions" for Transition Metal Catalysis. *Angew. Chem. Int. Ed.* **2000**, *39*, 3772-3789.

(36) Matsumoto, K.; Hwang, J.; Kaushik, S.; Chen, C.-Y.; Hagiwara, R. Advances in Sodium Secondary Batteries Utilizing Ionic Liquid Electrolytes. *Energ. Environ. Sci.* **2019**, *12*, 3247-3287.

(37) Yin, H.; Han, C.; Liu, Q.; Wu, F.; Zhang, F.; Tang, Y. Recent Advances and Perspectives on the Polymer Electrolytes for Sodium/Potassium-Ion Batteries. *Small* **2021**, *17*, 2006627.

(38) Mun, J.; Yim, T.; Choi, C. Y.; Ryu, J. H.; Kim, Y. G.; Oh, S. M. Linear-Sweep Thermammetry Study on Corrosion Behavior of Al Current Collector in Ionic Liquid Solvent. *Electrochem. Solid-State Lett.* **2010**, *13*, A109-A111.

(39) Cho, E.; Mun, J.; Chae, O. B.; Kwon, O. M.; Kim, H.-T.; Ryu, J. H.; Kim, Y. G.; Oh, S. M. Corrosion/Passivation of Aluminum Current Collector in Bis(Fluorosulfonyl)Imide-Based Ionic Liquid for Lithium-Ion Batteries. *Electrochem. commun.* **2012**, *22*, 1-3.

(40) Kühnel, R.-S.; Lübke, M.; Winter, M.; Passerini, S.; Balducci, A. Suppression of Aluminum Current Collector Corrosion in Ionic Liquid Containing Electrolytes. *J. Power Sources* **2012**, *214*, 178-184.

(41) Allen, J. L.; McOwen, D. W.; Delp, S. A.; Fox, E. T.; Dickmann, J. S.; Han, S.-D.; Zhou, Z.-B.; Jow, T. R.; Henderson, W. A. N-Alkyl-N-Methylpyrrolidinium Difluoro(Oxalato)Borate Ionic

Liquids: Physical/Electrochemical Properties and Al Corrosion. *J. Power Sources* **2013**, *237*, 104-111.

(42) Liu, C.; Ma, X.; Xu, F.; Zheng, L.; Zhang, H.; Feng, W.; Huang, X.; Armand, M.; Nie, J.; Chen, H.; Zhou, Z. Ionic Liquid Electrolyte of Lithium Bis(Fluorosulfonyl)Imide/N-Methyl-N-Propylpiperidinium Bis(Fluorosulfonyl)Imide for Li/Natural Graphite Cells: Effect of Concentration of Lithium Salt on the Physicochemical and Electrochemical Properties. *Electrochim. Acta* **2014**, *149*, 370-385.

(43) Vogl, T.; Menne, S.; Balducci, A. Mixtures of Protic Ionic Liquids and Propylene Carbonate as Advanced Electrolytes for Lithium-Ion Batteries. *Phys. Chem. Chem. Phys.* **2014**, *16*, 25014-25023.

(44) Theivaprakasam, S.; Girard, G.; Howlett, P.; Forsyth, M.; Mitra, S.; MacFarlane, D. Passivation Behaviour of Aluminium Current Collector in Ionic Liquid Alkyl Carbonate (Hybrid) Electrolytes. *NPJ Mater. Degrad.* **2018**, *2*, 13.

(45) Liu, Q.; Dzwiniel, T. L.; Pupek, K. Z.; Zhang, Z. Corrosion/Passivation Behavior of Concentrated Ionic Liquid Electrolytes and Its Impact on the Li-Ion Battery Performance. *J. Electrochem. Soc.* **2019**, *166*, A3959-A3964.

(46) Hwang, J.; Matsumoto, K.; Hagiwara, R. Electrolytes toward High-Voltage Na3v2(Po4)2f3 Positive Electrode Durable against Temperature Variation. *Adv. Energy Mater.* **2020**, *10*, 2001880.

(47) Onuma, H.; Kubota, K.; Muratsubaki, S.; Hosaka, T.; Tatara, R.; Yamamoto, T.; Matsumoto, K.; Nohira, T.; Hagiwara, R.; Oji, H.; Yasuno, S.; Komaba, S. Application of Ionic Liquid as K-Ion Electrolyte of Graphite//$K_2Mn[Fe(Cn)_6]$ Cell. *ACS Energy Letters* **2020**, *5*, 2849-2857.

(48) Otaegui, L.; Goikolea, E.; Aguesse, F.; Armand, M.; Rojo, T.; Singh, G. Effect of the Electrolytic Solvent and Temperature on Aluminium Current Collector Stability: A Case of Sodium-Ion Battery Cathode. *J. Power Sources* **2015**, *297*, 168-173.

(49) Hwang, J.; Aoyagi, I.; Takiyama, M.; Matsumoto, K.; Hagiwara, R. Inhibition of Aluminum Corrosion with the Addition of the Tris (Pentafluoroethyl) Trifluorophosphate Anion to a Sulfonylamide-Based Ionic Liquid for Sodium-Ion Batteries. *J. Electrochem. Soc.* **2022**, *169*, 080522.

(50) Doughty, D. H.; Roth, E. P. A General Discussion of Li Ion Battery Safety. *Electrochem. Soc. Interface* **2012**, *21*, 37.

(51) Chen, Y.; Kang, Y.; Zhao, Y.; Wang, L.; Liu, J.; Li, Y.; Liang, Z.; He, X.; Li, X.; Tavajohi, N.; Li, B. A Review of Lithium-Ion Battery Safety Concerns: The Issues, Strategies, and Testing Standards. *Journal of Energy Chemistry* **2021**, *59*, 83-99.

(52) Lin, X.; Salari, M.; Arava, L. M. R.; Ajayan, P. M.; Grinstaff, M. W. High Temperature Electrical Energy Storage: Advances, Challenges, and Frontiers. *Chem. Soc. Rev.* **2016**, *45*, 5848-5887.

(53) Feng, Y.; Zhou, L.; Ma, H.; Wu, Z.; Zhao, Q.; Li, H.; Zhang, K.; Chen, J. Challenges and Advances in Wide-Temperature Rechargeable Lithium Batteries. *Energ. Environ. Sci.* **2022**, *15*, 1711-1759.

(54) Earle, M. J.; Mcauley, B. J.; Ramani, A.; Seddon, K. R.; Thomson, J. M. Metal Bis-Triflimide Compounds and Methods for Synthesis of Metal Bis-Triflimide Compounds. United States **2006**.

(55) Krummacher, J.; Balducci, A. $Al(TFSI)_3$ as a Conducting Salt for High-Voltage Electrochemical Double-Layer Capacitors. *Chem. Mater.* **2018**, *30*, 4857-4863.

(56) Krummacher, J.; Hess, L.; Balducci, A. $Al(TFSI)_3$ in Acetonitrile as Electrolytes for Electrochemical Double Layer Capacitors. *J. Electrochem. Soc.* **2019**, *166*, A1763.

(57) Ma, T.; Xu, G.-L.; Li, Y.; Wang, L.; He, X.; Zheng, J.; Liu, J.; Engelhard, M. H.; Zapol, P.; Curtiss, L. A.; Jorne, J.; Amine, K.; Chen, Z. Revisiting the Corrosion of the Aluminum Current Collector in Lithium-Ion Batteries. *J. Phys. Chem. Lett.* **2017**, *8*, 1072-1077.

(58) Morita, M.; Shibata, T.; Yoshimoto, N.; Ishikawa, M. Anodic Behavior of Aluminum in Organic Solutions with Different Electrolytic Salts for Lithium Ion Batteries. *Electrochim. Acta* **2002**, *47*, 2787-2793.

(59) Peng, C.; Yang, L.; Zhang, Z.; Tachibana, K.; Yang, Y.; Zhao, S. Investigation of the Anodic Behavior of Al Current Collector in Room Temperature Ionic Liquid Electrolytes. *Electrochim. Acta* **2008**, *53*, 4764-4772.

(60) Mousavi, M. P.; Wilson, B. E.; Kashefolgheta, S.; Anderson, E. L.; He, S.; Buhlmann, P.; Stein, A. Ionic Liquids as Electrolytes for Electrochemical Double-Layer Capacitors: Structures That Optimize Specific Energy. *ACS Appl. Mater. Interfaces* **2016**, *8*, 3396-3406.

(61) Kunze, M.; Jeong, S.; Paillard, E.; Schönhoff, M.; Winter, M.; Passerini, S. New Insights to Self-Aggregation in Ionic Liquid Electrolytes for High-Energy Electrochemical Devices. *Adv. Energy Mater.* **2011**, *1*, 274-281.

(62) Garcia, B.; Armand, M. Aluminium Corrosion in Room Temperature Molten Salt. *J. Power Sources* **2004**, *132*, 206-208.

(63) Kotronia, A.; Asfaw, H. D.; Tai, C.-W.; Hahlin, M.; Brandell, D.; Edström, K. Nature of the Cathode–Electrolyte Interface in Highly Concentrated Electrolytes Used in Graphite Dual-Ion Batteries. *ACS Appl. Mater. Interfaces* **2021**, *13*, 3867-3880.

(64) Xue, W.; Shi, Z.; Huang, M.; Feng, S.; Wang, C.; Wang, F.; Lopez, J.; Qiao, B.; Xu, G.; Zhang, W. FSI-Inspired Solvent and "Full Fluorosulfonyl" Electrolyte for 4 V Class Lithium-Metal Batteries. *Energ. Environ. Sci.* **2020**, *13*, 212-220.

(65) Kerner, M.; Plylahan, N.; Scheers, J.; Johansson, P. Ionic Liquid Based Lithium Battery Electrolytes: Fundamental Benefits of Utilising Both TFSI and FSI Anions? *Phys. Chem. Chem. Phys.* **2015**, *17*, 19569-19581.

(66) Pham, T. D.; Bin Faheem, A.; Kim, J.; Oh, H. M.; Lee, K.-K. Practical High-Voltage Lithium Metal Batteries Enabled by Tuning the Solvation Structure in Weakly Solvating Electrolyte. *Small* **2022**, *18*, 2107492.

(67) Yamada, Y.; Chiang, C. H.; Sodeyama, K.; Wang, J.; Tateyama, Y.; Yamada, A. Corrosion Prevention Mechanism of Aluminum Metal in Superconcentrated Electrolytes. *ChemElectroChem* **2015**, *2*, 1687-1694.

(68) Wang, R.; Li, W.; Liu, L.; Qian, Y.; Liu, F.; Chen, M.; Guo, Y.; Liu, L. Carbon Black/Graphene-Modified Aluminum Foil Cathode Current Collectors for Lithium Ion Batteries with Enhanced Electrochemical Performances. *J. Electroanal. Chem.* **2019**, *833*, 63-69.

(69) Hosaka, T.; Matsuyama, T.; Kubota, K.; Tatara, R.; Komaba, S. Kfsa/Glyme Electrolytes for 4 V-Class K-Ion Batteries. *J. Mater. Chem. A* **2020**, *8*, 23766-23771.

(70) Rath, P. C.; Wang, Y.-W.; Patra, J.; Umesh, B.; Yeh, T.-J.; Okada, S.; Li, J.; Chang, J.-K. Composition Manipulation of Bis(Fluorosulfonyl)Imide-Based Ionic Liquid Electrolyte for High-Voltage Graphite//$LiNi_{0.5}Mn_{1.5}O_4$ Lithium-Ion Batteries. *Chem. Eng. J.* **2021**, *415*, 128904.

For Table of Contents Only